Bioelectrochemistry 122 (2018) 213–220

Contents lists available at ScienceDirect

Bioelectrochemistry

journal homepage: www.elsevier.com/locate/bioelechem

Growth and current production of mixed culture anodic biofilms remain unaffected by sub-microscale surface roughness

Mélanie Pierra [a], Mehdi Golozar [b,c], Xu Zhang [a], Antonin Prévoteau [a], Michael De Volder [b,c], Dominiek Reynaerts [b], Korneel Rabaey [a,*]

[a] Center for Microbial Ecology and Technology (CMET), Ghent University, Belgium
[b] Department of Mechanical Engineering, University of Leuven, Member Flanders Make, Leuven, Belgium
[c] Department of Engineering, University of Cambridge, Cambridge, UK

ARTICLE INFO

Article history:
Received 31 December 2017
Received in revised form 4 April 2018
Accepted 6 April 2018
Available online 12 April 2018

Keywords:
Surface topography
Roughness
Bioelectrochemical systems (BESs)
Electroactive biofilms (EABs)
Mixed culture
Micro electrodischarge machining (micro-EDM)

ABSTRACT

Bioelectrochemical systems couple electricity demand/supply to the metabolic redox reactions of microorganisms. Generally, electrodes act not only as electron acceptors/donors, but also as physical support for an electroactive biofilm. The microorganism-electrode interface can be modified by changing the chemical and/or topographical features of the electrode surface. Thus far, studies have reported conflicting results on the impact of the electrode surface roughness on the growth and current production of biofilms. Here, the surface roughness of the glassy carbon electrodes was successfully modified at the sub-microscale using micro electrodischarge machining, while preserving the surface chemistry of the parent glassy carbon. All microbial electrodes showed similar startup time, maximum current density, charge transport ability across the biofilm and biomass production. Interestingly, an increase in the average surface cavity depth was observed for the biofilm top layer as a function of the electrode surface roughness (from 7 μm to 16 μm for a surface roughness of 5 nm to 682 nm, respectively). These results indicated that the surface roughness at a sub-microscale does not significantly impact the attachment or current production of mixed culture anodic biofilms on glassy carbon. Likely earlier observations were associated with changes in surface chemistry, rather than surface topography.

1. Introduction

During the past two decades, microbial fuel cells and more generally bioelectrochemical systems (BESs) have attracted much interest. In particular, several studies have focused on the anodic electroactive biofilms (EABs), which can carry out direct electron transfer between the electroactive bacteria and electrodes [1,2]. *Via* this mode of transfer, higher current densities can be obtained without the need for redox mediator addition. The projected current densities generated by electroactive biofilms (EABs) have increased from a few amperes per square meter in the early 2000s to now >100 A/m^2 using high specific surface area electrodes [3,4].

In the anodic compartment of BESs, bacteria oxidize organic compounds and use conductive solids as terminal electron acceptors [5,6]. These electrodes act not only as the electron acceptor, but also as the support material on which the bacterial films grow. Both microorganisms and electrodes constitute the core engine of BESs. Therefore, the optimization of a functional microorganism-electrode interface is a key step to build an efficient BES. Similar to most biofilm-based bioprocesses, the microbial attachment, biomass production and mass transfer of the soluble substrates and product within the biofilm have to be favorable to optimize the process [7].

The general process of biofilm formation on a surface follows successive steps [8]. First, the bacteria are brought in contact with the surface due to gravitational or hydrodynamic forces. The movement of bacteria toward and on the surface is facilitated by flagella, fimbriae and pili [8]. The attachment is facilitated by negatively charged cell-surface in case of an adhesion to the anode [9]. Second, the bacteria adhere to the surface. This adhesion step is highly dependent on the properties of the material surface. Surface chemical and topographical features, including macro-, micro- and nanoscale structures play an important role in this step. Third, the bacteria proliferate on the surface and synthesize the three-dimensional biofilm matrix – *i.e.* maturation step. Finally, a mature biofilm is obtained based on the specific bacterial physiology and metabolism of the organisms in the biofilm. However, at the maturation stage, bacteria can detach from the biofilm. This is due, in general biofilm cycles, to a change in environment conditions of the biofilm (*e.g.* nutrient depletion).

In the case of EABs, the choice of the electrode material is a key step to promote biocompatibility and an efficient heterogeneous electron transfer at the biofilm-electrode interface. In recent years, there has

* Corresponding author.
E-mail address: Korneel.rabaey@ugent.be (K. Rabaey).

https://doi.org/10.1016/j.bioelechem.2018.04.002
1567-5394/

been an ever-growing interest in electrode materials for BESs. In general and because they are particularly biocompatible, carbon based materials are used for the growth of EABs [9,10] and chemical modification can further improve their efficacy [11]. Metals (particularly stainless steel) and composite materials (metals and carbon) are used as well [9]. A large variety of carbon-based materials have been used as substrate for microbial anode including carbon plates, cloth, paper, felt, brush, foam, reticulated vitreous carbon and carbon nanotubes [9]. Three-dimensional, porous electrodes are particularly favorable for this application because they provide a higher specific surface area for the attachment of EABs [9,12]. Furthermore, nanoscale surface features can affect the cell behavior and increase microbial retention [13]. Processing highly ordered microscale patterns on flat surfaces may in fact be the most suitable approach to investigate the impact of intrinsic submicrotopography on biofilm structure and current production.

So far, the impact of roughness on EABs has mainly been studied on stainless steel electrodes. Pons et al. reported a significant impact of stainless steel electrode roughness on the formation of pure culture *Geobacter sulfurreducens* biofilms on a cathode. By increasing the surface roughness R_a from 2.0 μm to 4.0 μm, they increased the maximum current density by a factor of 1.6 [14]. In contrast, it has been found that a surface roughness of 5 μm on stainless steel did not significantly affect the current output of a mixed culture anodic biofilm compared to a smooth electrode [15]. More recently, a study on anodic biofilms on gold nano-rough electrodes (up to 4,5 nm), focusing on the early stages of biofilm attachment shown an increase of current densities due to the roughness (from 0,9 to 2,5 $A \cdot m^{-2}$ for resp smooth and 4,5 nm rough electrodes) despite an erratic colonization occurs, with bacteria clusters of the electrode. More generally, for non-electroactive biofilms, Flint et al. postulated that microbial adhesion is favored by entrapment of the bacteria in the cavities of the surfaces that exhibit an average roughness value (R_a) in the range of the microbial cell size (*i.e.* approx. a few μm) [16]. According to this hypothesis, Hilbert et al. showed no effect of submicron roughness ($R_a < 0.9$ μm) on bacterial adhesion on stainless steel with pure cultures of *Pseudomonas* sp., *Listeria monocytogenes* and *Candida lipolytica* [17].

In this study, we investigated the impact of three sub-microscale surface roughness topographies on mixed culture anodic biofilms in terms of biomass attachment, current production and biofilm structure. For this study, we used biocompatible glassy carbon materials. We modified the topography of the glassy carbon electrodes using a micro electrodischarge machining (micro-EDM) system. The electrode surfaces were characterized in terms of roughness, chemistry and hydrophobicity. The biofilms were grown on the electrodes by chronoamperometry in a multichannel electrodes system. The biofilms were finally characterized in terms of hydrated biovolume and biofilm topography by confocal microscopy.

2. Materials and methods

2.1. Surface roughness modification of glassy carbon electrodes

SIGRADUR® G grade glassy carbon electrodes (HTW Hochtemperatur-Werkstoffe GmbH, Thierhaupten, Germany) were used to investigate the microbial colonization, biofilm formation and performance in terms of current density and charge transport parameters as a function of surface roughness. A SARIX® SX-100-HPM micro-EDM system with a rotating tungsten carbide electrode was employed to introduce a range of submicroscale roughness topographies on the surfaces of the glassy carbon electrodes. Micro-EDM is a contactless micromanufacturing process based on an electro-thermal principle, where a voltage is applied between the tungsten carbide and glassy carbon electrodes submerged in a dielectric medium resulting in the formation of a series of discrete microplasma discharges that act as a heat source on the surface of the glassy carbon electrode [18–20]. In general, the thermoelectric energy generated in the discharge gap between the two electrodes is responsible for the local heating, (partial) melting and evaporation, and the subsequent removal of the glassy carbon material [18–22]. To produce different surface topographies, the machining settings were chosen within both finishing and roughing regimes predefined by the manufacturer using the combination of electrical parameters (pulse duration, pulse frequency, current and potential) and technological parameters (discharge gap, discharge energy, gain and regulation). Three different sub-microscale surface topographies were produced with ascending order of roughness: low (L), medium (M) and high (H) roughness machining settings corresponding to the energy index *e* of 13, 105 and 365, respectively. The energy index *e* is predefined by the manufacturer and is related to the generator capacitance. The wear compensation factor was also adjusted specifically for each energy index *e* to enable continuous and effective removal of the workpiece material [23,24]. Prior to bioelectrochemical studies, the electrodes were thoroughly cleaned using acetone and deionized water in an ultrasonic bath. As received glassy carbon electrodes were also used as control (C) materials.

2.2. Surface physicochemical characterization of the electrodes

Scanning Electron Microscopy (*SEM*) was performed with a LEO GEMINI 1530VP FEG-SEM system to evaluate the surface roughness topography of untreated and treated glassy carbon electrodes. The operating voltage and working distance were 8 kV and 5 mm, respectively. The samples were sufficiently conductive that additional coating was not necessary. *Energy Dispersive X-ray Spectroscopy* (*EDX*) (FEI Nova NanoSEM™ 450 FEG-SEM) was used under EDX mode to carry out the local elemental analysis of the free surfaces of untreated and treated glassy carbon electrodes. The operating voltage and working distance were 15 kV and 5 mm, respectively. The samples were sufficiently conductive that additional coating was not required. *White Light Interferometry* (Veeco Wyko NT3300 Optical Profiler) was employed to investigate the roughness of the free surfaces of untreated and treated glassy carbon electrodes. Two surface roughness parameters R_a (roughness average) and R_z (ten-point average maximum profile) were measured to describe their surface topographies. The 2D/3D surface topographies of all glassy carbon electrodes were also examined. *Visible Raman Spectroscopy* (EZRAMAN-N-532-B1S) was used with a laser wavelength 532 nm (FWHM = 5 nm) as the excitation source to examine the surfaces of untreated and treated glassy carbon electrodes. *Drop Shape Analysis* (*DSA*) (DSA100 KRÜSS) was used with a sessile drop method to measure the static contact angle of the droplets on the free surfaces of untreated and treated glassy carbon electrodes. Deionized water was used with the droplet volume of 10 μL and dispensing rate of 180.1 $\mu L \cdot min^{-1}$. A 30-s contact time was adopted to ensure the equilibrium angle was reached prior to taking the measurements. The measurements were subsequently presented as an average of the left and right contact angles of a static droplet (in equilibrium). Prior to measurements, the electrodes were cleaned with acetone and deionized water using a sonicator followed by thorough drying.

2.3. Bioelectrochemical system

The EABs were grown on electrodes in two custom-made two-compartment BES reactors previously described by Guo et al. [11] (Fig. 1). This reactor design allows to simultaneous testing of eight working electrodes (WE) per reactor with one counter electrode (SS mesh cathode) and one reference electrode (Ag/AgCl 3 M KCl). The 2 × 2 cm square shaped glassy carbon electrodes were connected to the reactor with an insulated copper wire fixed on the back of the plate with silver paint. The back and side planes of the plates were then insulated with epoxy glue (ThorLabs - TS10). For each reactor, three WE roughnesses were tested in duplicates, and two WEs were kept as smooth controls. All electrochemical experiments were conducted with a CHI 1000C Multi-Potentiostat (CH Instruments, Austin, TX, U.S.A.). Uncompensated resistances (Fig. S1) between each WE and the reference electrode were assessed by applying current interruption

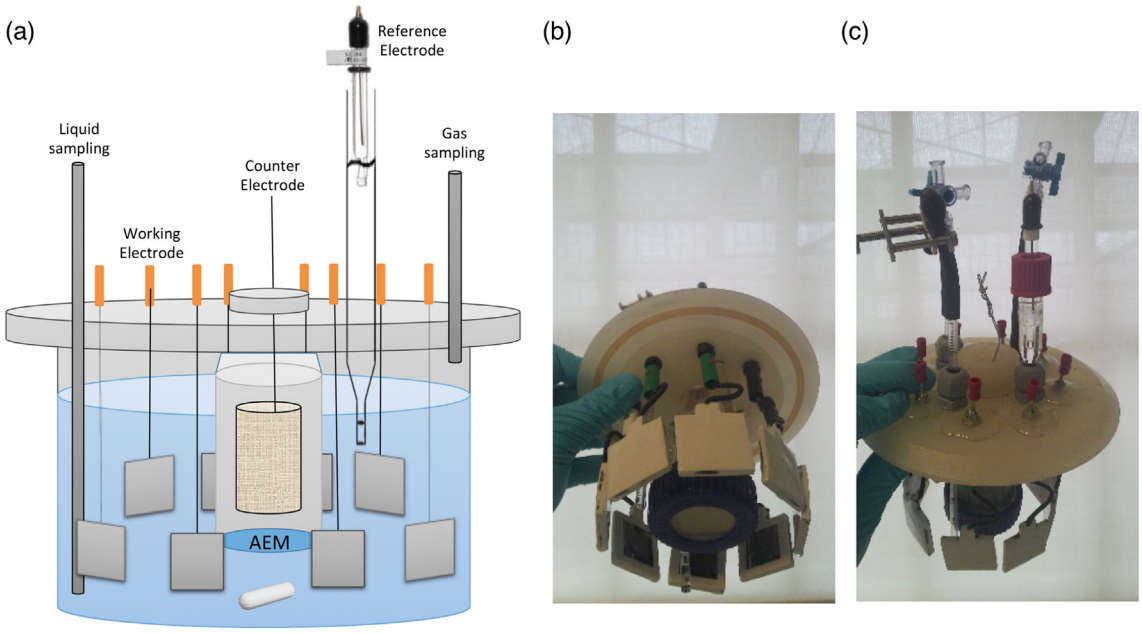

Fig. 1. Reactor design. This disposal contains 8 glassy carbon working electrodes, a stainless-steel mesh as a counter electrode and a reference electrode (Ag/AgCl). (a) Scheme of the reactor. (b) Photo of the 8 glassy carbon electrodes surrounding the counter electrode compartment. (c) Photo from the top of the reactor.

method as previously described [25]. The anodic chamber was filled with 450 mL of modified M9 medium (pH = 7) [26] with 2 $g \cdot L^{-1}$ (24 mM) sodium acetate as the electron donor. Before inoculation, the medium was sparged for 30 min with nitrogen gas to ensure anaerobic condition. The reactor was inoculated with 50 mL fresh anodic effluent from an existing acetate-fed BES reactor. The cathodic chamber was filled with 50 mL M9 buffer medium. The potential of each anode was set to −0.2 V *vs.* Ag/AgCl and current generation was recorded by chronoamperometry (CA). The anolyte was continuously stirred with a magnetic stirrer at 350 rpm. Experiments were conducted in the dark at 28 °C in a temperature-controlled room. At the end of each of the 3 cycles (when acetate was consumed and the current density decreased), cyclic voltammetry (CV) was performed on all biofilms in the same medium under turnover condition (with acetate). The CVs were performed within a potential window between −0.8 V to 0.2 V *vs.* Ag/AgCl at a scan rate of 10 $mV \cdot s^{-1}$. The charge transport parameter across the EABs ($C \times D_{app}^{1/2}$, where C is the average concentration of redox centers involved in the conduction – assuming 1 electron per redox center – and D_{app} is the apparent diffusion coefficient for the electrons across the EAB) was determined under turnover conditions by double potential step chronoamperometry (DPSC) as previously described [25].

2.4. Biofilm characterization

After growth, the biofilms were prepared for confocal staining as previously described [27]. The biofilms were washed twice with 10 mM PBS buffer. Biofilms were fixed with 2.5% glutaraldehyde in 10 mM phosphate buffer (pH 7.3) for 30 min at 4 °C. They were subsequently incubated in the dark in staining mix for 15 min. The live/dead staining mixture consisted of 1.5 $\mu L \cdot mL^{-1}$ of SYTO9 (green) and propidium iodide (red) (Live/Dead BacLight Bacterial Viability Kits, Life Technologies) in PBS buffer. The biofilms were incubated in PBS buffer for 15 min in the dark to remove excess stain. Then, excess liquid was evaporated for a few minutes. Before the biofilms were completely dry, mounting medium, prepared with 9 mL glycerol, 1 mL 1 M Tris HCl buffer at pH 8.3, 0.05 g n-propyl gallate, heated till all powder was dissolved, was applied on the biofilms. The biofilms were covered with a cover slide, which was sealed with nail polish, and kept at −20 °C in the dark. Afterwards, the stained biofilms were visualized and Z-stacks were captured by using a confocal laser scanning microscope (CLSM, Nikon C1, The Netherlands). Three areas were observed per biofilm with a 40× lens. CLSM image data were processed using ImageJ software and the COMSTAT plugin for biovolume calculation [28,29]. The top surface of the biofilms was analyzed by measuring the sum of the surface coverage percentage of the 10 first Z-stacks on the surface of the biofilms, *i.e.* the top 20 μm of the surface of the biofilms.

3. Results

3.1. Electrode surface modification and characterization

Three different roughnesses were produced on the surfaces of the glassy carbon electrodes using the micro-EDM process. Fig. 2(a) shows the R_a (roughness average) and R_z (ten-point average maximum profile) roughness values obtained for untreated and treated glassy carbon electrodes using white light interferometry. The power settings of the micro-EDM process were gradually increased to obtain surfaces with increasing roughness [30]. The R_a (R_z) values increased from 5.1 ± 1.0 nm (0.1 ± 0.1 μm) for untreated electrodes to 198.3 ± 19.1 nm (2.2 ± 0.2 μm), 347.6 ± 15.5 nm (3.3 ± 0.2 μm) and 681.6 ± 127.8 nm (5.3 ± 0.7 μm) for treated electrodes with low, medium and high roughness machining settings, respectively. Fig. 2(a) also shows the 2D/3D surface profiles of the electrodes exhibiting an initial surface waviness associated with the untreated electrodes, which was subsequently transformed into rougher sub-microscale surface topographies using micro-EDM. In addition to the optical surface profiles, the SEM images of the treated electrodes showed the uniform formation and distribution of signature surface craters caused by the local heating, (partial) melting and evaporation of the glassy carbon electrode within the discharge gap, Fig. 2(b). The average size of the craters appeared to increase with increasing the roughness machining settings, and with the inside of the craters exhibiting a relatively smoother finish compared to their periphery, as shown in the insets. It is also noteworthy that larger craters obtained at higher power settings of the micro-EDM process appeared to contain smaller craters. Moreover, Fig. 2(c) presents the contact angle measurements carried out on the free surfaces of untreated and treated glassy carbon electrodes. Although the contact

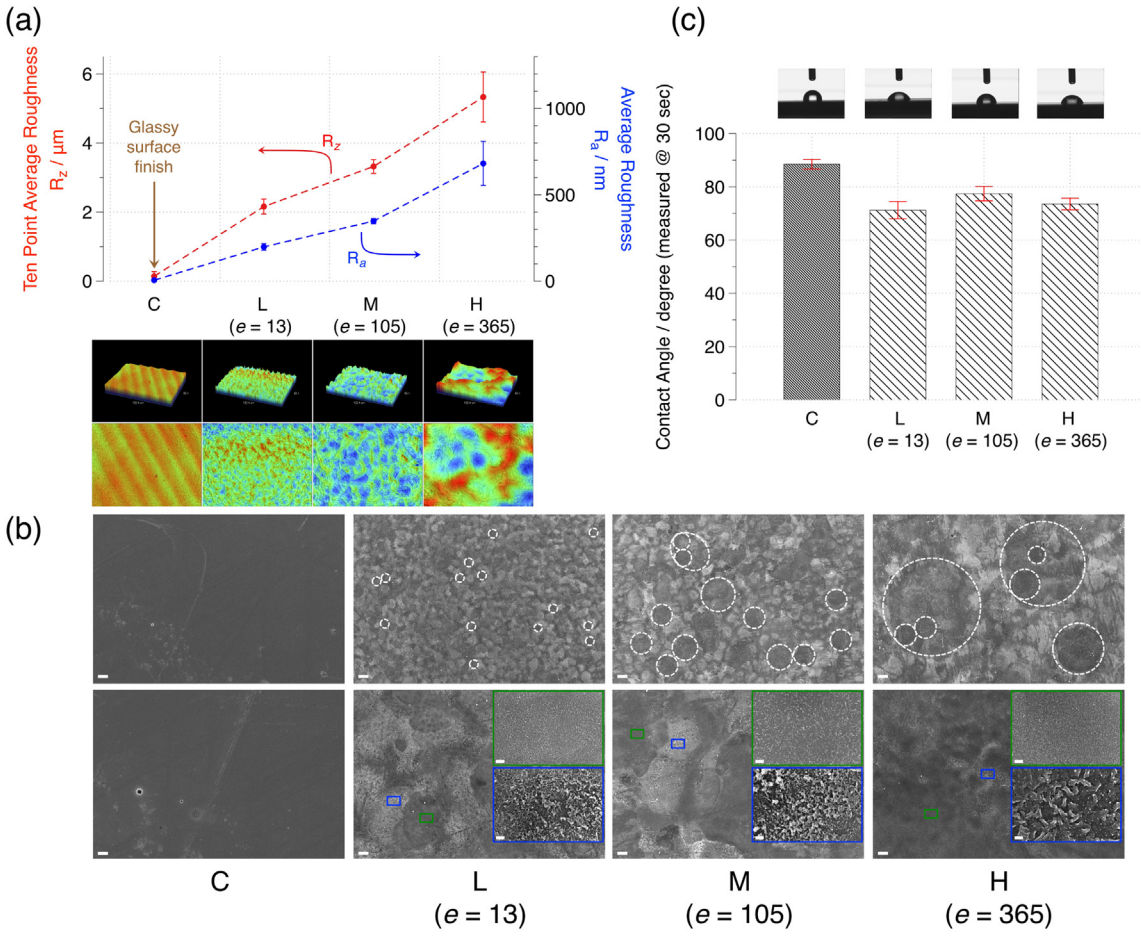

Fig. 2. Surface physical properties of untreated (control) and treated glassy carbon electrodes: surface roughness measurements and roughness topography using white light interferometry, (a), scanning electron micrographs of the surface morphology illustrating the uniform formation and distribution of signature surface craters with dotted circles highlighting the average size of the craters and that they increase with the power settings of the micro-EDM process (top row scale bar: 10 µm; bottom row scale bar: 2 µm; bottom row inset scale bar: 200 nm), (b), and contact angle measurements, (c). C = control, L = low roughness machining settings used during micro-EDM, M = medium roughness machining settings used during micro-EDM, H = high roughness machining settings used during micro-EDM, and e = energy index used during micro-EDM.

angles were slightly decreased from 88.5° ± 1.8° for untreated electrodes to 71.2° ± 3.2°, 77.4° ± 2.7° and 73.6° ± 2.2° for treated electrodes with low, medium and high roughness machining settings, respectively, micro-EDM did not present a significant impact on the hydrophilic properties of the electrodes.

Fig. 3 presents the chemical analyses of the free surfaces of untreated and treated glassy carbon electrodes using EDX and Raman spectroscopy. The EDX spectra showed that the free surfaces of all electrodes consisted purely of carbon, verifying that no impurities were incorporated onto the electrodes surface during the micro-EDM process. For instance, no traces from the tungsten carbide electrode used in the micro-EDM process were detected on the surface. Furthermore, the Raman signature of a typical sp^2-bonded carbon material was observed for all untreated and treated glassy carbon electrodes. The Raman spectra illustrated the presence of

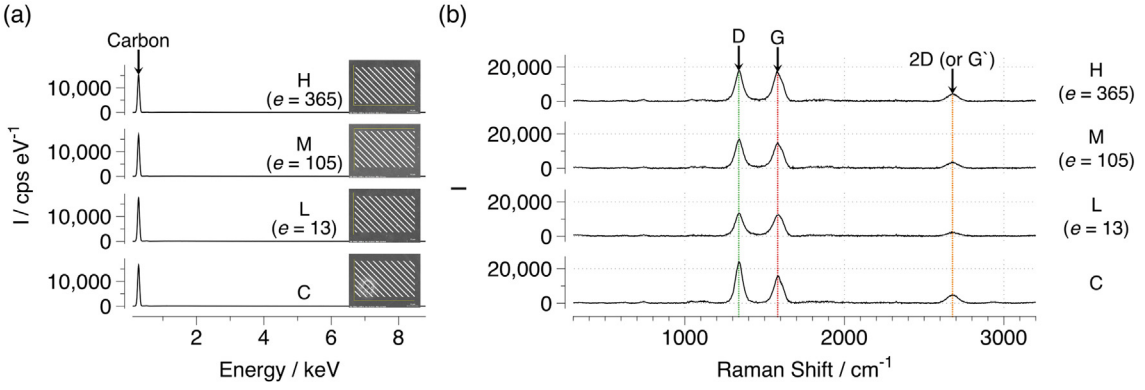

Fig. 3. Surface chemical properties of untreated (control) and treated glassy carbon electrodes: energy dispersive X-ray spectroscopy of all electrodes confirming the presence of pure carbon electrode materials, (a), Raman spectroscopy showing the Raman signature of a typical sp^2-bonded carbon material with G, D and 2D Raman peaks for all untreated and treated glassy carbon electrodes, (b). C = control, L = low roughness machining settings used during micro-EDM, M = medium roughness machining settings used during micro-EDM, H = high roughness machining settings used during micro-EDM, and e = energy index used during micro-EDM.

a typical G peak (~1582 cm^{-1}) corresponding to the E_{2g} phonon (quantum of energy or quasiparticle that here in the case of an inelastic scattering of photons (Raman) is associated with the vibration of the crystal lattice), which is due to the primary in-plane vibrational mode of the sp^2 carbon atoms [31–38]. All electrodes also showed the presence of a primary D peak (~1338 cm^{-1}) together with its second-order overtone, 2D peak (~2676 cm^{-1}). The D peak is linked to structural disorders and therefore requires defects for activation while the 2D peak is typically always present — although their origin is not yet clearly understood [31–38]. The D and 2D Raman peak positions are dispersive and dependent on the excitation energy (laser wavelength) [37,38].

3.2. Bioelectrocatalytic performance

Fig. 4 illustrates the current density output as a function of time for all untreated (control) and treated glassy carbon electrodes in Reactor #1. All curves represent the average current of two replicate electrodes. These chronoamperometric curves exhibited a similar trend for all untreated and treated electrodes, with similar maximum current densities with respect to their projected surface area (0.51 ± 0.10 $mA \cdot cm^{-2}$). These results show that the current density output was not affected by the sub-microscale surface roughness topographies of glassy carbon anodes. Interestingly, the surface roughness was found to have slightly influenced the onset of current production, where it had delayed the current onset of treated rough glassy carbon electrodes in comparison to the untreated (control) electrodes. The control electrodes started to generate a current density of minimum 10 μA cm^{-2} at about 31 ± 1.5 h just before the rough electrodes at about 38 ± 1.5 h – this suggested that surface roughness may have slightly affected the initial attachment of bacteria.

3.3. Characterization of electro-active biofilms

Fig. S2 shows the cyclic voltammograms (CV) of the EABs on all untreated (controls) and treated glassy carbon electrodes. The resulting CVs were comparable to those reported in previous studies for both mixed cultures dominated *Geobacter* spp. and pure culture *Geobacter sulfurreducens* biofilms [39].

Fig. 5 presents the confocal microscopy images of the EABs for all untreated and treated glassy carbon electrodes. Fig. 6 presents the biovolume of the biofilms. The average maximal thicknesses of the biofilms were 30 ± 8 μm, 39 ± 5 μm, 30 ± 10 μm and 31 ± 5 μm for untreated glassy carbon electrodes, L, M and H, respectively. This showed an excellent reproducibility across all electrodes. The biovolume (μm^3), in terms of the average biovolume per unit of the projected area of the electrode (μm^2), varied between 27.95 ± 6.69 μm^3 for H and 39.33 ± 6.36 μm^3 for L. Finally, the thickness and the biovolume results showed that the sub-microscale roughness topography of the anodes presented no significant impact on the biovolume of the biofilms.

The 3D confocal images of the biofilms showed the presence of cavities on the surface of the biofilms, Figs. S3 and S4. The average biofilm surface cavity depth increased slightly from 7.4 ± 0.4 μm for the untreated glassy carbon electrodes to 15.5 ± 0.5 μm for the electrodes with the highest surface roughness, H.

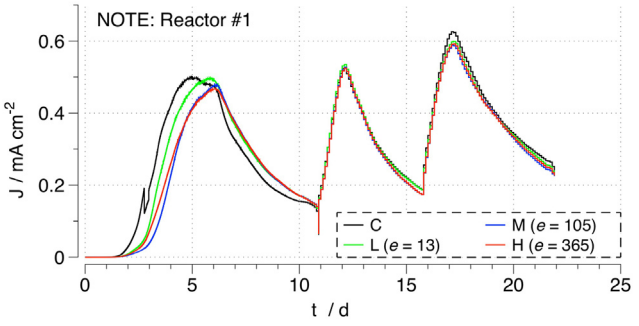

Fig. 4. Representative chronoamperograms recorded for electrodes of different roughnesses. Obtained from reactor #1.

4. Discussion

4.1. Sub-microscale surface roughness does not impact the attachment of bacteria to the glassy carbon anodes in mixed culture

According to Flint et al., the size of the electrode surface features should be similar to the bacteria to favor entrapment of the microorganisms and/or to provide them with suitable anchoring sites [16]. At a smaller scale, it has been assumed that bacteria could distort to increase the contact of the microbial surface close to the biofilm support, *i.e.* the electrode in the present case [8,13]. This phenomenon would imply an increase in binding energy expense for bacteria [13], as microbial surface deformation costs elastic energy. Therefore, such surface features could cause an energy cost to bacteria and decrease the biofilm electroactivity. This could reduce the ability of the bacteria to attach to the nanoscale surface features, limit the possibilities for bacteria to sense the surfaces and prevent them from attachment [13]. However, evidence of this still has to be revealed with bacteria. Therefore, bacterial ability to respond to sub-microscale surface features could be less efficient than on a smooth surface. Furthermore, the cell membrane features could contribute to the attachment of bacteria to the electrode as already shown in previous studies with other bacteria and archaea [40,41]. Due to their small size and their motility, the bacterial cell membrane features, including flagella and pili, would play an important role in this context.

4.2. Sub-microscale surface roughness does not impact biofilm biovolume and current production

Several studies observed an increase of current production of microbial electrodes by adding or forming nanoscale features on the surface [11,12]. In the particular case of nanoparticle addition, not only the surface topography, but also the chemistry is modified. The increase in the specific surface area together with the chemical modification of the surface may have contributed to the increase in current production. In our study we used micro-EDM that offers a unique ability to modify the roughness of glassy carbon electrodes in a controlled fashion without altering their surface chemistry.

Our results indicated that the electrochemical performance and the volume of biofilm attached per projected area are not substantially affected by the sub-microscale surface roughness of the glassy carbon electrodes. Previous studies with pure cultures highlighted an increase of surface current production due to surface roughness. Ye et al. showed that increasing the surface roughness of glassy carbon electrodes from 10 nm to 100 nm in pure cultures significantly enhanced *Shewanella oneidensis* biofilm electrochemical performance [42]. At a higher microscale level, increasing the surface roughness from 2 μm to 4 μm increased the current by a factor of 1.6 for *Geobacter sulfurreducens* on a cathode [14]. Such high roughness values at the microscale level were achieved by sandblasting the surface of the electrodes and the biofilm was obtained *via* polarizing the electrodes for 8 days (only during the early stages of the biofilm development), whereas in our study we easily obtained a thick mature biofilm after 3 cycles with successive additions of 24 mM acetate. Additionally, although *Geobacter sulfurreducens* is considered a model bacterium for anodic biofilms, Pons et al. used it as a microbial cathode, which requires other metabolic pathways. Moreover, contrary to the aforementioned studies, Pocaznoi et al. reported that surface roughness of 5 μm produced on stainless steel electrodes did not impact the current output of mixed culture biofilms [15].

Our findings on the lack of impact at the sub-microscale level are in accordance with an earlier study reported by Pocaznoi et al., who worked with mixed cultures on stainless steel surfaces with roughness

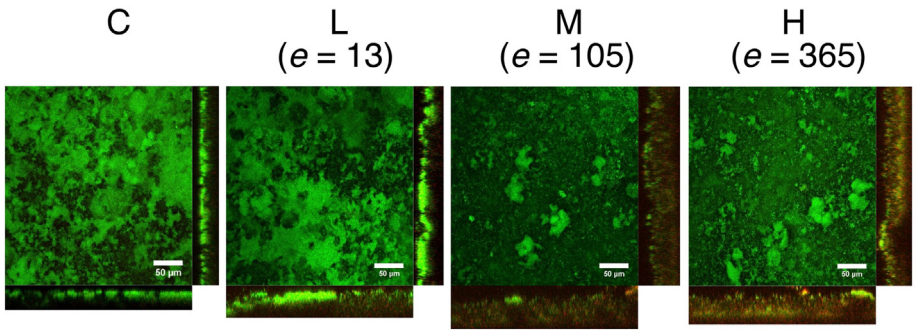

Fig. 5. Confocal laser scanning microscopy images of EABs. The images show the top of the biofilms and two cross sections of the EABs grown on the control electrode and electrodes L, M and H.

ranging from smooth to 5 µm [15]. However, our study focused on a smaller sub-microscale roughness (<1 µm) on glassy carbon surfaces. Taken together, these studies strongly suggest that modifying the surface roughness of electrodes at a sub-microbial-scale would not lead to higher current production.

4.3. Sub-microscale surface roughness does not impact the electron transfer across biofilms

We used double potential step chronoamperometry (Fig. 7) to determine the charge transport parameter ($C \times D_{app}^{1/2}$) for the different EABs. Their values are very similar regardless of the electrode surface roughness, and they are comparable to previous studies [25]. Notably, the charge transport parameter ($C \times D_{app}^{1/2}$) appeared to be slightly lower for the untreated (control) electrodes compared to the rough treated electrodes. As the composition, charge density, hydrophobic/hydrophilic and lipophobic/lipophilic nature of a surface, the roughness could also have influenced biofilm functioning [9,43]. No significant impact of sub-microscale surface roughness ranging from 198.3 ± 19.1 nm to 681.6 ± 127.8 nm was observed on the electron transfer across biofilms. Increasing the roughness range might be interesting for future studies to assess the impact of roughness on the charge transport parameter.

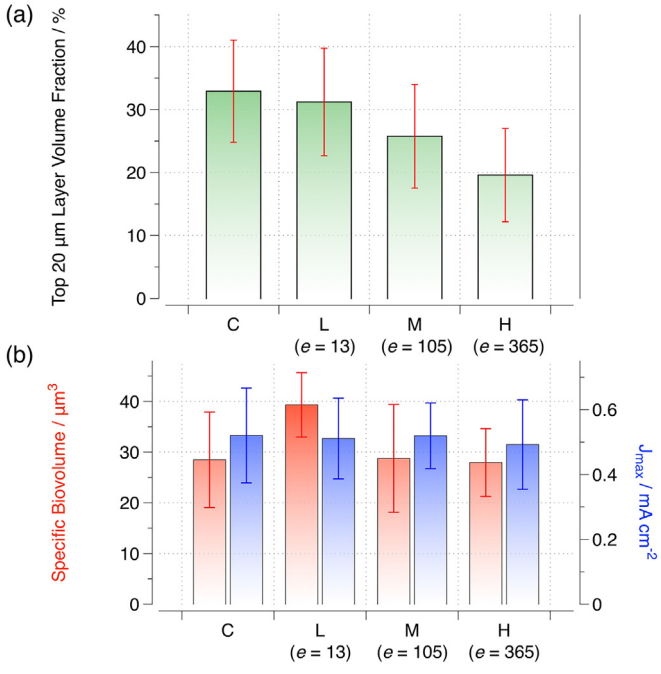

Fig. 6. Biofilms characterizations and current densities. (a) Top 20 µm layer volume fraction (%) corresponding to the top 20 µm of the biofilm surface. The percentage of the biovolume decreases while roughness was increased, highlighting the appearance of pits on the highest roughness produced on the glassy carbon electrodes. (b) Average maximal current density for each electrode roughness tested in the 2 reactors, and specific biovolume (per unit of projected µm² on the electrode) obtained for each roughness tested. Error bars representing two standard deviations (n = 6). The specific biomass was calculated with the program COMSTAT (plugin added to ImageJ).

4.4. Sub-microscale surface roughness impacted the biofilm surface topography

The calculation of the total percentage coverage of the first 10 stacks of the confocal biofilm images (*i.e.* first 20 µm) on top of the biofilm, showed a decrease of the Top 20 µm layer volume fraction with the increase of the roughness. This suggests the impact of a sub-microscale roughness on the topography of the biofilm surface. The measurement of the depth of those cavities obtained at the top of the biofilms showed that cavity depth can reach up to approx. 15 µm for the highest electrode roughness in comparison to approx. 7 µm for the control electrode (C) (Fig. S3). In a previous study, Pons et al. observed that roughness induced a clustering effect of microorganisms on the electrodes surface [14]. Considering the fact that the biofilm was 8 days old in the case of Pons et al., our results are in accordance with their work as the cavities and bumps obtained on the surface of the biofilms could be the result of an amplification of this phenomenon after several cycles of growth of the biofilm until a mature stage. Furthermore, Pons et al. studied a different range of roughness values (from 2 µm to 4 µm) and a cathodic biofilm with a *Geobacter sulfurreducens* pure culture, which is different from our study in mixed culture on an anode. Very recently, in the same research team, Champigneux et al. [44] shown that a nanoscale roughness (Ra = 4,5 nm) induced a colony patterning at the early stage of biofilm colonization on a pure culture *Geobacter sulfurreducens* anodic biofilm. More generally, it is established, with non-EAB, that aside from the surface chemistry, the sessile bacteria, during the adhesion, react to surface topography. Especially, at a macroscale level,

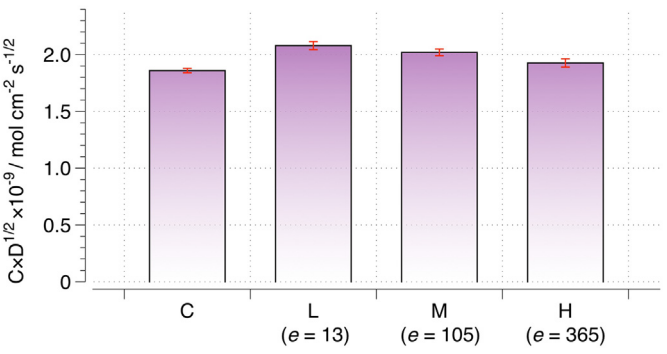

Fig. 7. Charge transport parameters of the EABs. The value ($C \times D_{app}^{1/2}$) illustrates the ability of EABs to transport electron across their conductive matrix.

they adhere preferentially to the bottom of cracks rather than on outer surfaces [8]. Whitehead et al. showed that during the attachment phase, a number of bacteria are localized on or in the topographical features for surfaces pits from 200 nm to 2 μm [13]. This study showed that increased surface roughness would contribute to a clustering effect on an EAB that would not only affect the adhesion phase but also the mature biofilm configuration.

5. Conclusion

This study investigated the effect of several sub-microscale surface roughness topographies on a mixed culture anodic biofilm in terms of electroactive performance, biomass production and biofilm topography. Our results showed that bacterial attachment, current production, charge transport parameter and biomass formation are not affected by the sub-microscale surface roughness of glassy carbon electrodes. However, an impact was observed on the surface topography of the biofilms with the emergence of cavities at higher surface roughness values. Such surface cavities may be due to the bacterial clustering effect on the rough surfaces; yet, the physiological impact of this effect is still unclear.

Acknowledgements

Jo Philips is kindly acknowledged for helping with confocal analysis. Silvia Hidalgo is kindly acknowledged for helping with image analyses. Melanie Pierra and Mehdi Golozar acknowledge the financial support by the Research Foundation – Flanders (FWO) under grant agreement No. G018814N. Xu Zhang is financially supported by the China Scholarship Council (File No. 201406120043). Antonin Prévoteau and Korneel Rabaey are supported by the European Research Council *via* Starter Grant ELECTROTALK. MdV is supported by the European Research Council *via* Starter Grant HIENA.

Appendix A. Supplementary data

Supplementary data to this article can be found online at https://doi.org/10.1016/j.bioelechem.2018.04.002.

References

[1] D.R. Bond, D.R. Lovley, Electricity production by *Geobacter sulfurreducens* attached to electrodes, Appl. Environ. Microbiol. 69 (2003) 1548–1555, https://doi.org/10.1128/AEM.69.3.1548.
[2] S.K. Chaudhuri, D.R. Lovley, Electricity generation by direct oxidation of glucose in mediatorless microbial fuel cells, Nat. Biotechnol. 21 (2003) 1229–1232, https://doi.org/10.1038/nbt867.
[3] G. He, Y. Gu, S. He, U. Schröder, S. Chen, H. Hou, Effect of fiber diameter on the behavior of biofilm and anodic performance of fiber electrodes in microbial fuel cells, Bioresour. Technol. 102 (2011) 10763–10766, https://doi.org/10.1016/j.biortech.2011.09.006.
[4] S. Chen, G. He, Q. Liu, F. Harnisch, Y. Zhou, Y. Chen, M. Hanif, S. Wang, X. Peng, H. Hou, U. Schröder, Layered corrugated electrode macrostructures boost microbial bioelectrocatalysis, Energy Environ. Sci. 2 (2012) 9769–9772, https://doi.org/10.1039/c2ee23344d.
[5] K. Rabaey, W. Verstraete, Microbial fuel cells: novel biotechnology for energy generation, Trends Biotechnol. 23 (2005) 291–298, https://doi.org/10.1016/j.tibtech.2005.04.008.
[6] B.E. Logan, K. Rabaey, Conversion of wastes into bioelectricity and chemicals by using microbial electrochemical technologies, Science (80-.) 337 (2012) 686–690, https://doi.org/10.1126/science.1217412.
[7] J.N. Wilking, V. Zaburdaev, M. De Volder, R. Losick, M.P. Brenner, D.A. Weitz, Liquid transport facilitated by channels in Bacillus subtilis biofilms, Proc. Natl. Acad. Sci. U. S. A. 110 (2013) 848–852, https://doi.org/10.1073/pnas.1216376110.
[8] K. Anselme, P. Davidson, A.M. Popa, M. Giazzon, M. Liley, L. Ploux, The interaction of cells and bacteria with surfaces structured at the nanometre scale, Acta Biomater. 6 (2010) 3824–3846, https://doi.org/10.1016/j.actbio.2010.04.001.
[9] K. Guo, A. Prévoteau, S.A. Patil, K. Rabaey, Engineering electrodes for microbial electrocatalysis, Curr. Opin. Biotechnol. 33 (2015) 149–156, https://doi.org/10.1016/j.copbio.2015.02.014.
[10] C. Santoro, M. Guilizzoni, J.P. Correa Baena, U. Pasaogullari, A. Casalegno, B. Li, S. Babanova, K. Artyushkova, P. Atanassov, The effects of carbon electrode surface properties on bacteria attachment and start up time of microbial fuel cells, Carbon N. Y. 67 (2014) 128–139, https://doi.org/10.1016/j.carbon.2013.09.071.
[11] K. Guo, B. Donose, A.H. Soeriyadi, A. Prévoteau, S.A. Patil, S. Freguia, J.J. Gooding, K. Rabaey, Flame oxidation of stainless steel felt enhances anodic biofilm formation and current output in bioelectrochemical systems, Environ. Sci. Technol. 48 (2014) 7151–7156, https://doi.org/10.1021/es500720g.
[12] L. Jourdin, S. Freguia, B.C. Donose, J. Chen, G.G. Wallace, J. Keller, V. Flexer, A novel carbon nanotube modified scaffold as an efficient biocathode material for improved microbial electrosynthesis, J. Mater. Chem. A 2 (2014) 13093–13102, https://doi.org/10.1039/C4TA03101F.
[13] K.A. Whitehead, J. Verran, The effect of surface topography on the retention of microorganisms, Food Bioprod. Process. 84 (2006) 253–259, https://doi.org/10.1205/fbp06035.
[14] L. Pons, M.L. Délia, A. Bergel, Effect of surface roughness, biofilm coverage and biofilm structure on the electrochemical efficiency of microbial cathodes, Bioresour. Technol. 102 (2011) 2678–2683, https://doi.org/10.1016/j.biortech.2010.10.138.
[15] D. Pocaznoi, A. Calmet, L. Etcheverry, B. Erable, A. Bergel, Stainless steel is a promising electrode material for anodes of microbial fuel cells, Energy Environ. Sci. 5 (2012) 9645–9652, https://doi.org/10.1039/C2EE22429A.
[16] S.H. Flint, J.D. Brooks, P.J. Bremer, Properties of the stainless steel substrate, influencing the adhesion of thermo-resistance streptococci, J. Food Eng. 43 (2000) 235–242.
[17] L.R. Hilbert, D. Bagge-Ravn, J. Kold, L. Gram, Influence of surface roughness of stainless steel on microbial adhesion and corrosion resistance, Int. Biodeterior. Biodegrad. 52 (2003) 175–185, https://doi.org/10.1016/S0964-8305(03)00104-5.
[18] K. Liu, B. Lauwers, D. Reynaerts, Process capabilities of micro-EDM and its applications, Int. J. Adv. Manuf. Technol. 47 (2010) 11–19, https://doi.org/10.1007/s00170-009-2056-1.
[19] D.T. Pham, S.S. Dimov, S. Bigot, A. Ivanov, K. Popov, Micro-EDM - recent developments and research issues, J. Mater. Process. Technol. 149 (2004) 50–57, https://doi.org/10.1016/j.jmatprotec.2004.02.008.
[20] S. Mahendran, R. Devarajan, T. Nagarajan, A. Majdi, A Review of Micro-EDM, Imecs, 2010 (doi:978-988-18210-4-1).
[21] J. Wang, F. Yang, J. Qian, D. Reynaerts, Study of alternating current flow in micro-EDM through real-time pulse counting, J. Mater. Process. Technol. 231 (2016) 179–188, https://doi.org/10.1016/j.jmatprotec.2015.12.010.
[22] J. Qian, F. Yang, J. Wang, B. Lauwers, D. Reynaerts, Material removal mechanism in low-energy micro-EDM process, CIRP Ann. Manuf. Technol. 64 (2015) 225–228, https://doi.org/10.1016/j.cirp.2015.04.040.
[23] J. Wang, J. Qian, E. Ferraris, D. Reynaerts, Precision micro-EDM milling of 3D cavities by incorporating in-situ pulse monitoring, Procedia CIRP 42 (2016) 656–661, https://doi.org/10.1016/j.procir.2016.02.297.
[24] J. Wang, J. Qian, E. Ferraris, D. Reynaerts, In-situ process monitoring and adaptive control for precision micro-EDM cavity milling, Precis. Eng. 47 (2017) 261–275, https://doi.org/10.1016/j.precisioneng.2016.09.001.
[25] X. Zhang, J. Philips, H. Roume, K. Guo, K. Rabaey, A. Prévoteau, Rapid and quantitative assessment of redox conduction across electroactive biofilms via double potential step chronoamperometry, ChemElectroChem (2017)https://doi.org/10.1002/celc.201600853.
[26] K. Guo, S. Freguia, P.G. Dennis, X. Chen, B.C. Donose, J. Keller, J.J. Gooding, K. Rabaey, Effects of surface charge and hydrophobicity on anodic biofilm formation, community composition, and current generation in bioelectrochemical systems, Environ. Sci. Technol. 47 (2013) 7563–7570.
[27] J. Philips, K. Rabaey, D.R. Lovley, M. Vargas, Biofilm formation by *Clostridium ljungdahlii* is induced by sodium chloride stress: experimental evaluation and transcriptome analysis, PLoS One 12 (2017)https://doi.org/10.1371/journal.pone.0170406.
[28] M. Vorregaard, Comstat2 - A Modern 3D Image Analysis Environment for Biofilms (PhD Thesis) http://www2.imm.dtu.dk/pubdb/views/edoc_download.php/5628/pdf/imm5628.pdf 2008.
[29] A. Heydorn, A. Heydorn, A.T. Nielsen, A.T. Nielsen, M. Hentzer, M. Hentzer, Quantification of biofilm structures by the novel computer program, Image Process. 146 (2000) 2395–2407, https://doi.org/10.1099/00221287-146-10-2395.
[30] A. Sabur, A. Moudood, M.Y. Ali, M.A. Maleque, Investigation of surface roughness in micro-electro discharge machining of nonconductive ZrO_2 for MEMS application, IOP Conf. Ser. Mater. Sci. Eng. 53 (2013), 012090. https://doi.org/10.1088/1757-899X/53/1/012090.
[31] A.C. Ferrari, Raman spectroscopy of graphene and graphite: disorder, electron-phonon coupling, doping and nonadiabatic effects, Solid State Commun. 143 (2007) 47–57, https://doi.org/10.1016/j.ssc.2007.03.052.
[32] A.C. Ferrari, J. Robertson, Interpretation of Raman spectra of disordered and amorphous carbon, Phys. Rev. B 61 (2000) 14095–14107, https://doi.org/10.1103/PhysRevB.61.14095.
[33] A.C. Ferrari, J. Robertson, Raman spectroscopy of amorphous, nanostructured, diamond-like carbon, and nanodiamond, Philos. Transact. A Math. Phys. Eng. Sci. 362 (2004) 2477–2512, https://doi.org/10.1098/rsta.2004.1452.
[34] Y. Wang, D.C. Alsmeyer, R.L. Mccreery, Raman spectroscopy of carbon materials: structural basis of observed spectra, Carbon N. Y. (1990) 557–563, https://doi.org/10.1021/cm00011a018.
[35] A.C. Ferrari, J. Robertson, Resonant Raman spectroscopy of disordered, amorphous, and diamondlike carbon, Phys. Rev. B 64 (2001), 075414. https://doi.org/10.1103/PhysRevB.64.075414.
[36] N.A. Solopova, N. Dubrovinskaia, L. Dubrovinsky, Raman spectroscopy of glassy carbon up to 60 GPa, Appl. Phys. Lett. 102 (2013) 1–5, https://doi.org/10.1063/1.4798660.
[37] A.C. Ferrari, D.M. Basko, Raman spectroscopy as a versatile tool for studying the properties of graphene, Nat. Publ. Group 8 (2013) 235–246, https://doi.org/10.1038/nnano.2013.46.

[38] M.S. Dresselhaus, A. Jorio, R. Saito, Characterizing graphene, graphite, and carbon nanotubes by Raman spectroscopy, Annu. Rev. Condens. Matter Phys. 1 (2010) 89–108, https://doi.org/10.1146/annurev-conmatphys-070909-103919.
[39] S. Srikanth, E. Marsili, M.C. Flickinger, D.R. Bond, Electrochemical Characterization of *Geobacter sulfurreducens* Cells Immobilized on Graphite Paper Electrodes, 99, 2008 1065–1073, https://doi.org/10.1002/bit.21671.
[40] K.F. Jarrell, M. Stark, D.B. Nair, J.P.J. Chong, Flagella and pili are both necessary for efficient attachment of *Methanococcus maripaludis* to surfaces, FEMS Microbiol. Lett. 319 (2011) 44–50, https://doi.org/10.1111/j.1574-6968.2011.02264.x.
[41] S. Vatanyoopaisarn, A. Nazli, C.E.R. Dodd, C.E.D. Rees, W.M. Waites, Effect of flagella on initial attachment of *Listeria monocytogenes* to stainless steel effect of flagella on initial attachment of *Listeria monocytogenes* to stainless steel, Appl. Environ. Microbiol. 66 (2000) 860–863, https://doi.org/10.1128/AEM.66.2.860-863.2000. Updated.
[42] Z. Ye, J. Hou, M.W. Ellis, B. Behkam, Dependance of electrochemical performance on anode surface roughness in microbial fuel cellsAIChE Annual Meeting, 2012.
[43] A. Kumar, L.H.-H. Hsu, P. Kavanagh, F. Barrière, P.N.L. Lens, L. Lapinsonnière, J.H. Lienhard, V.U. Schröder, X. Jiang, D. Leech, The ins and outs of microorganism–electrode electron transfer reactions, Nat. Rev. Chem. 1 (2017) 0024, https://doi.org/10.1038/s41570-017-0024.
[44] P. Champigneux, C. Renault-Sentenac, D. Bourrier, C. Rossi, M.-L. Delia, A. Bergel, Effect of surface nano/micro-structuring on the early formation of microbial anodes with *Geobacter sulfurreducens*: experimental and theoretical approaches, Bioelectrochemistry (2018)https://doi.org/10.1016/j.bioelechem.2018.02.005.